STELLAR ASTROPHYSICS

A massive helium star with a sufficiently strong magnetic field to form a magnetar

Tomer Shenar[1]*†, Gregg A. Wade[2], Pablo Marchant[3], Stefano Bagnulo[4], Julia Bodensteiner[3,5], Dominic M. Bowman[3], Avishai Gilkis[6], Norbert Langer[7,8], André Nicolas-Chené[9], Lidia Oskinova[10], Timothy Van Reeth[3], Hugues Sana[3], Nicole St-Louis[11], Alexandre Soares de Oliveira[12], Helge Todt[10], Silvia Toonen[1]

Magnetars are highly magnetized neutron stars, the formation mechanism of which is unknown. Hot helium-rich stars with spectra dominated by emission lines are known as Wolf-Rayet stars. We observed the binary system HD 45166 using spectropolarimetry and reanalyzed its orbit using archival data. We found that the system contains a Wolf-Rayet star with a mass of 2 solar masses and a magnetic field of 43 kilogauss. Stellar evolution calculations indicate that this component will explode as a supernova, and that its magnetic field is strong enough for the supernova to leave a magnetar remnant. We propose that the magnetized Wolf-Rayet star formed by the merger of two lower-mass helium stars.

Neutron stars form in supernovae by the collapse of stellar cores that exceed the Chandrasekhar mass limit [mass $M \gtrsim 1.4$ solar masses ($M_\odot$)]. Bare stellar cores can be exposed as hot, evolved helium-rich stars that have shed their outer hydrogen-rich layers. A subset of these massive helium stars is observed as Wolf-Rayet stars, which have spectra dominated by broad emission lines produced by strong stellar winds (*1*, *2*). Massive helium stars (those with $M \gtrsim 1.4 M_\odot$) are thought to be stripped products of more massive stars that lost their hydrogen-rich envelopes through stellar winds, eruptions, or interactions with a binary companion (*3*, *4*). Alternatively, massive helium stars could be produced through the merger of lower-mass objects (*5*).

Approximately 10% of young neutron stars have magnetic fields $>10^{14}$ G (*6*). These are known as magnetars; their origin is debated (*7*, *8*). One formation scenario invokes fossil magnetic fields rooted in the massive core of a progenitor star that collapses during a supernova (*9*). About 7 to 10% of massive main-sequence stars have strong (several kG) large-scale surface magnetic fields (*10*, *11*); such stars could be progenitors of magnetars. However, corresponding magnetic fields have not been detected in evolved massive stars (*12*). Strongly magnetic low-mass helium stars have been observed (*13*–*15*), but not massive magnetic helium stars exceeding the Chandrasekhar limit.

The HD 45166 binary system (also cataloged as ALS 8946) comprises a main sequence star (classified as spectral type B7 V) with a hot stellar companion. The hot companion has a spectrum dominated by the characteristic emission lines of a Wolf-Rayet star (Fig. 1), but it is classified as a "quasi–Wolf-Rayet" (qWR) star owing to its peculiarly narrow emission lines (widths of hundreds of kilometers per second instead of the typical thousands); spectral variability; and the anomalous presence of strong carbon, oxygen, and nitrogen lines in its spectrum. Previous radial velocity (RV) measurements have shown a 1.6-day periodicity in the velocity of the B7 V component, which was interpreted as the orbital period of the system (*16*). This implied a mass of $4.2 \pm 0.7 M_\odot$ for the Wolf-Rayet component and a pole-on orbital configuration (inclination $i = 0.7°$) (*16*). That mass is well below the typical masses of Wolf-Rayet stars in the Milky Way [$M \gtrsim 8 M_\odot$ (*17*)]; no other massive helium stars are known with $M \lesssim 8 M_\odot$ (*18*). Comparison with stellar atmosphere models that do not assume local thermodynamic equilibrium (non-LTE models) has shown that the Wolf-Rayet component is a hot (surface effective temperature $T_* = 70$ kK), helium-rich star with enhanced nitrogen and carbon contents (compared with the composition of the Sun) (*19*). A latitude-dependent wind model can reproduce the spectrum of the Wolf-Rayet component (*19*); however, the implied mass-loss rate is orders of magnitude greater than predictions for helium stars of this mass (*20*–*22*).

The presence of a carbon and nitrogen emission-line complex in the range of 4430 to 4460 Å (known as the Of?p phenomenon) and strong spectral variability are typical indirect signatures of magnetism in hot

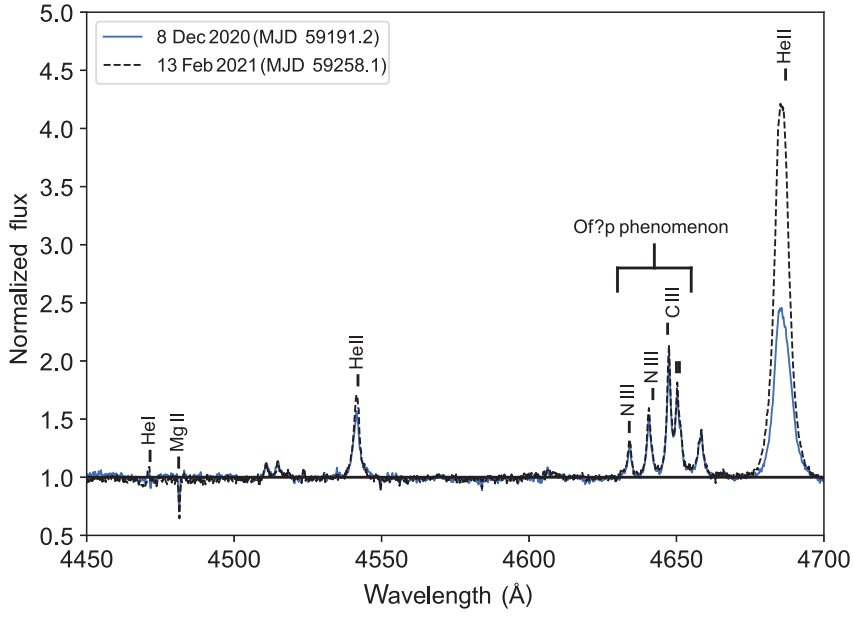

Fig. 1. Indications of possible magnetism in HD 45166. Solid blue and thin dashed black lines indicate two optical HERMES spectra of HD 45166 (*25*) taken ≈70 days apart (see legend). The thick black line indicates the continuum level. Labels indicate the Of?p phenomenon (*23*, *24*) and the He II line at 4686 Å, which is variable (also seen in Fig. 3). These are common features of hot magnetic stars, which indicates that the Wolf-Rayet component might be magnetic. The narrow Mg II ion line at 4481 Å is due to the B7 V component.

[1]Anton Pannekoek Institute for Astronomy, University of Amsterdam, 1098 XH Amsterdam, Netherlands. [2]Department of Physics and Space Science, Royal Military College of Canada, Kingston K7K7B4, Canada. [3]Institute of Astronomy, Katholieke Universiteit Leuven, 3001 Leuven, Belgium. [4]Armagh Observatory and Planetarium, College Hill, Armagh BT61 9DG, UK. [5]European Southern Observatory, 85748 Garching bei München, Germany. [6]The School of Physics and Astronomy, Tel Aviv University, Tel Aviv 6997801, Israel. [7]Argelander-Institut für Astronomie, Universität Bonn, 53121 Bonn, Germany. [8]Max-Planck-Institut für Radioastronomie, 53121 Bonn, Germany. [9]National Optical-Infrared Astronomy Research Laboratory, National Science Foundation, Hilo, Hawai'i 96720, USA. [10]Institut für Physik und Astronomie, Universität Potsdam, D-14476 Potsdam, Germany. [11]Département de physique, Université de Montréal, Montréal H2V 0B3, Canada. [12]Institute of Research and Development, Universidade do Vale do Paraíba, São José dos Campos 12244-000, Brazil.
*Corresponding author. Email: T.Shenar@uva.nl
†Present address: Centro de Astrobiología (Consejo Superior de Investigaciones Científicas - Instituto Nacional de Técnica Aeroespacial), 28850 Torrejón de Ardoz, Spain.

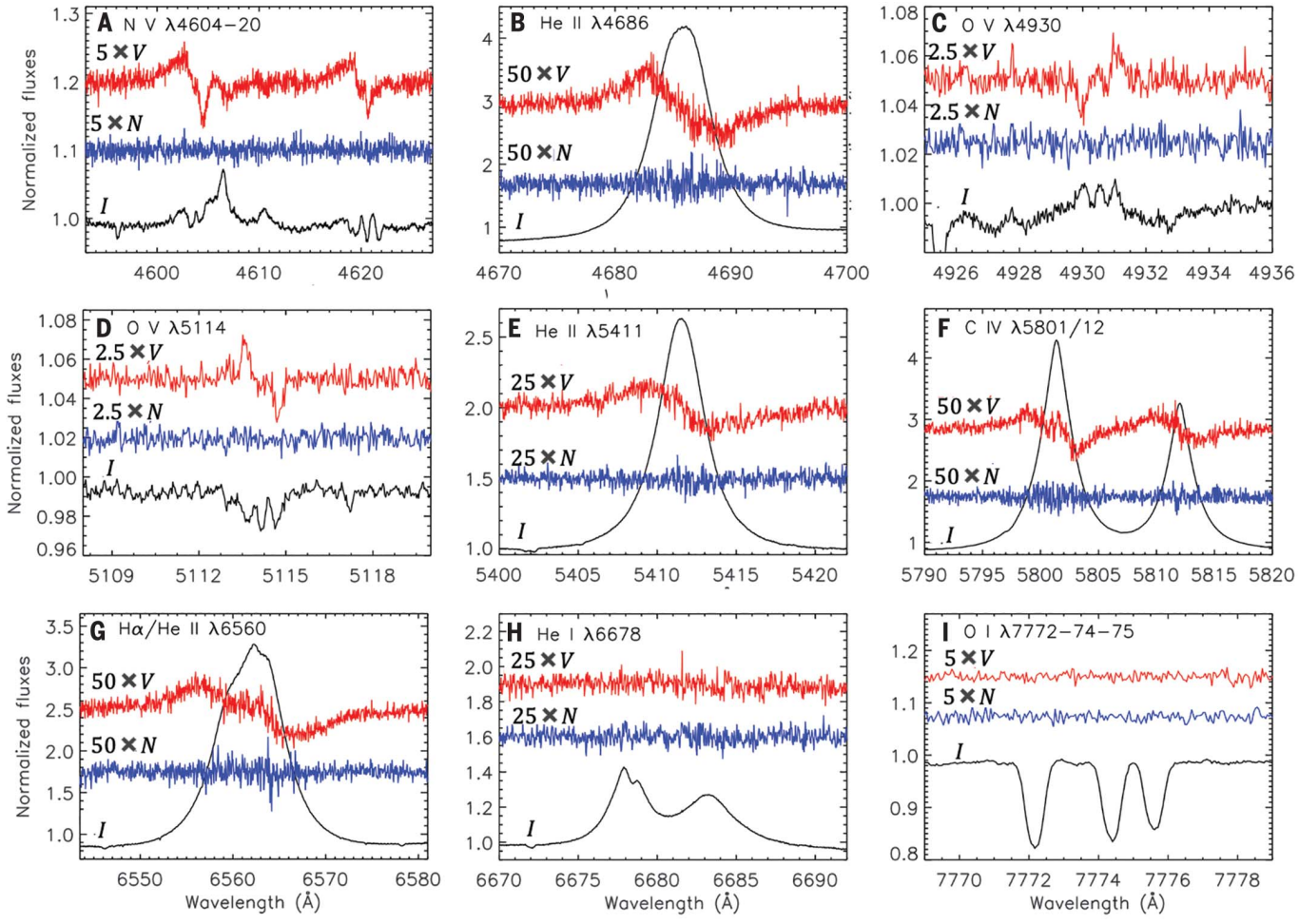

Fig. 2. Spectropolarimetry of HD 45166. (A) to (I) shows the intensity spectrum (Stokes *I*, black lines), diagnostic null spectrum (*N*, blue lines), and Stokes *V* spectrum (red lines) from the co-added ESPaDOnS spectrum. The *N* and *V* spectra have been vertically shifted and scaled for display purposes, by the factors listed in each graph. (**A** to **H**) Diagnostic lines of the Wolf-Rayet component. Zeeman splitting is visible in the O v lines at the λ4930 (C) and λ5114 (D), which are both because of O v. We used these lines to measure the magnetic field strength. (**I**) An O I (neutral oxygen ion) triplet associated with the B7 V star, which has no Stokes *V* signature.

stars (*23*, *24*). We used spectropolarimetry to investigate whether the Wolf-Rayet component in HD 45166 is magnetic.

Observations of HD 45166

We collected eight spectropolarimetric observations of HD 45166 in February 2022 using the Echelle Spectropolarimetric Device for the Observation of Stars (ESPaDOnS) spectropolarimeter on the Canada-France-Hawaii Telescope (CFHT) (*25*). The spectra measure the polarimeteric Stokes parameters *I* and *V* over the wavelength range 3668 to 10,480 Å at a resolving power of 65,000. We used them to measure the magnetic-field strength in the Wolf-Rayet and B7 V components of HD 45166.

We used archival spectra from three other instruments to measure RVs over a longer period (*25*). They were 103 spectra obtained with the Coudé spectrograph at the 1.6 m telescope of Laboratório Nacional de Astrofísica (LNA), mainly covering 4520 to 4960 Å; 36 spectra obtained with the Fiber-fed Extended Range Optical Spectrograph (FEROS) at the 1.52 m telescope of the European Southern Observatory (ESO), covering 3830 to 9215 Å; and 28 spectra acquired with the High-Efficiency and High-Resolution Mercator Echelle Spectrograph (HERMES) on the 1.2 m Mercator telescope, covering 3770 to 9000 Å. We used additional archival ultraviolet spectroscopy and photometric data to analyze the spectral energy distribution (SED) of the system (*25*).

Evidence for magnetism

We detected circular polarization (Stokes *V*) in the ESPaDOnS spectra for the majority of lines associated with the Wolf-Rayet component (Fig. 2). We also detected Zeeman splitting (doubling of spectral lines owing to a magnetic field) in two O v (quadruply ionized oxygen) lines (Fig. 2, C and D) that form in or close to the stellar surface. We measured the magnetic field from the separation of the split Zeeman components of these lines, finding a mean field modulus $\langle B \rangle_{\rm qWR} = 43.0 \pm 2.5$ kG and a mean longitudinal field $\langle B_z \rangle_{\rm qWR} = 13.5 \pm 2.5$ kG (table S1). The ratio between these values (approximately 3:1) is consistent with a dipolar magnetic field viewed near the magnetic pole (*26*).

Such a strong magnetic field in the Wolf-Rayet component implies that its emission-line spectrum is formed in the star's magnetosphere (the region containing plasma confined by the magnetic field loops), not in a radially expanding stellar wind (*25*). If so, one-dimensional (1D) stellar atmosphere models [as used in previous studies (*19*)] are not appropriate for the emission lines, thus affecting the previously derived physical parameters.

Stellar parameters

We reanalyzed the spectra and SED using PoWR, a non-LTE model atmosphere code optimized for Wolf-Rayet stars (*27*, *28*). Because the PoWR code is also 1D, we only used it to

analyze spectral features that originate in the stellar surface of the Wolf-Rayet component, not emission lines from the magnetosphere (*25*). The resulting physical parameters are listed in table S1. We found an effective temperature for the Wolf-Rayet component of $T_* = 56.0 \pm 5.0$ kK, which is ≈15 kK lower than previously determined (*19*). The effective temperature and bolometric luminosity L [we found $\log(L/L_\odot) = 3.830 \pm 0.050$, where $L_\odot$ is the luminosity of the Sun] indicate that the magnetic Wolf-Rayet component is not a main sequence star, but an evolved object.

We applied the same analysis to the B7 V component (*25*) then input the resulting stellar parameters into BONNSAI, a Bayesian tool for comparing observations to stellar models (*29*). That analysis indicates that the mass and age of the B7 V component are $M_B = 3.38 \pm 0.10\ M_\odot$ and 105 ± 35 million years (Myr), respectively (table S1).

The Wolf-Rayet component exhibits changes in line strength, including as the He II (doubly ionized helium) line at 4686 Å. These appear to be periodic (Fig. 3A), with a best-fitting period of 124.8 days (Fig. 3B). Periodic changes in the line strengths of hot magnetic stars are typically interpreted as their rotational periods (*30*, *31*), implying a rotational period $P_{\mathrm{rot,qWR}} = 124.8 \pm 0.2$ days for the Wolf-Rayet component. This period is consistent with the narrow O V lines, which have a projected rotational velocity $v \sin i \lesssim 10$ kms^{-1}.

Binary orbit

The ESPaDOnS spectra indicate that the B7 V component exhibits spectral line profile variations caused by nonradial gravity-mode pulsations (fig. S9). We performed a frequency analysis of an optical light curve obtained with the Transiting Exoplanet Survey Satellite (TESS), which detects several periods, including 1.6 days (*25*). We therefore concluded that the 1.6-day period previously attributed to orbital motion (*16*) is instead caused by pulsations in the B7 V component. We reassessed the binary orbit and the mass of the Wolf-Rayet component M_{qWR} under this interpretation.

To determine the orbit, we analyzed all the RV data, which span 24 years (*25*). We found a long-term antiphase motion of the B7 V and Wolf-Rayet components (Fig. 4). There are multiple RV periodicities associated with both the Wolf-Rayet and B7 V components (*25*). We adopted the best-fitting orbit (table S1), which has an orbital period P = 8200 ± 190 days and a semimajor axis a = 10.5 ± 1.8 astronomical units (au). This indicates that the components are much more widely separated than had previously been determined.

The orbital solution indicates a mass ratio of $q \equiv M_{\mathrm{qWR}}/M_B = 0.60 \pm 0.13$. Combining this with the mass of the B7 V component ($M_B = 3.38 \pm 0.10\ M_\odot$) derived from the BONNSAI analysis implies $M_{\mathrm{qWR}} = 2.03 \pm 0.44\ M_\odot$ (uncertainties are 68% confidence intervals). This is less than the 4.2 $M_\odot$ previously reported, but still above the Chandrasekhar limit.

The derived mass and luminosity of the qWR component are consistent with mass-luminosity relations for helium stars (*32*). The large separation and implied orbital inclination of $i = 49 \pm 11°$ [derived from $M_B \sin^3 i$ and M_B (table S1)] explain the low-amplitude RV motion of both binary components, without invoking a pole-on configuration.

Implications for magnetar formation

With a mass of $2.03 \pm 0.44\ M_\odot$, we expect the Wolf-Rayet component to evolve until it collapses into a neutron star. We calculated evolutionary models of the system, which are consistent with this interpretation, although the final fate of the Wolf-Rayet component is sensitive to uncertainties in the model (*25*). During core collapse, magnetic flux conservation causes an increase in the magnetic field at the surface. With a stellar radius of $R_{*,\mathrm{qWR}} = 0.88 \pm 0.16 R_\odot$ (where $R_\odot$ is the radius of the Sun), calculated with the Stefan-Boltzmann relation, our measured $\langle B \rangle_{\mathrm{qWR}} = 43.0 \pm 2.5$ kG, and assuming a final neutron-star radius of 12 km (*33*), we calculate the expected magnetic field of the neutron star to be $\langle B \rangle_{\mathrm{NS}} = (1.11 \pm 0.42) \times 10^{14}$ G. This is within the range observed for magnetars [$\langle B \rangle \gtrsim 10^{14}$ G (*34*)]. Our observations and stellar-evolution models therefore indicate that the

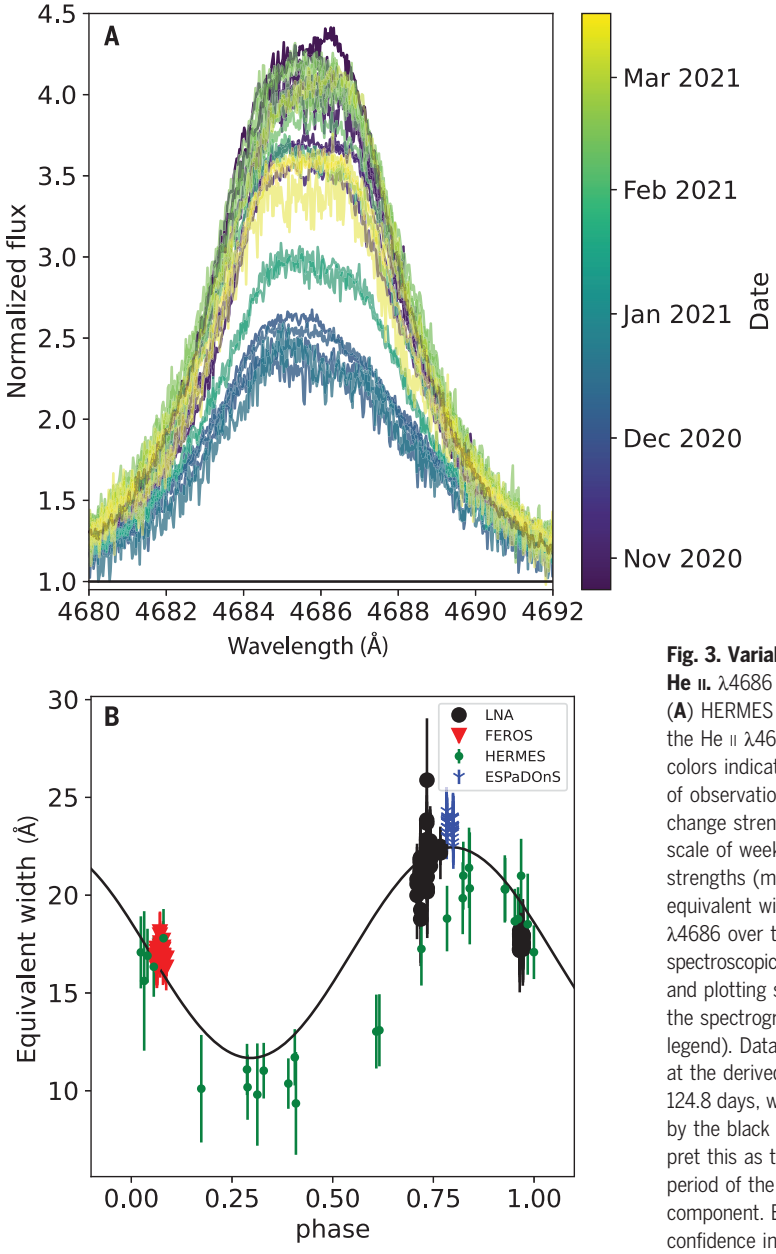

Fig. 3. Variability of the He II λ4686 emission line. (**A**) HERMES spectra of the He II λ4686 line, with colors indicating the date of observation. The lines change strength on a timescale of weeks. (**B**) Line strengths (measured as equivalent widths) of He II λ4686 over the 24-year spectroscopic dataset. Colors and plotting symbols indicate the spectrograph used (see legend). Data were phased at the derived period of 124.8 days, which is indicated by the black curve. We interpret this as the rotational period of the Wolf-Rayet component. Error bars are confidence intervals of 1σ.

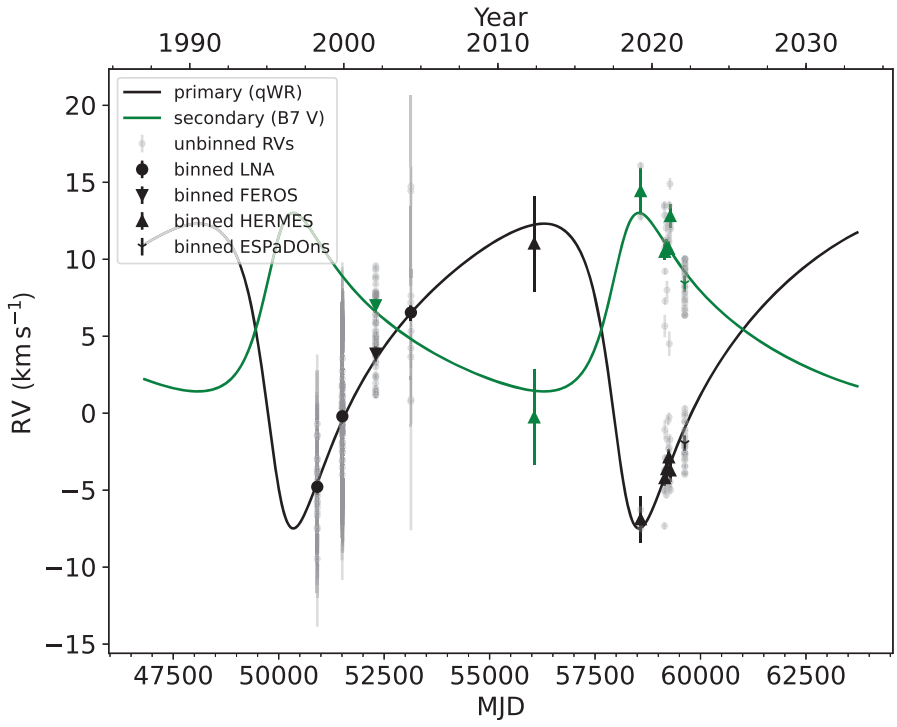

Fig. 4. Two-component orbital solution for HD 45166. RVs of the Wolf-Rayet and B7 V components are plotted in gray, with green and black symbols indicating the same data binned by 30 days for the Wolf-Rayet and B7 V components, respectively. Plotting symbols indicate the instruments used (see legend). Solid lines are the best-fitting RV curves for the Wolf-Rayet (black) and B7 V (green) components. The model fit has a reduced χ^2 of 1.21. Error bars are confidence intervals of 1 σ (*25*).

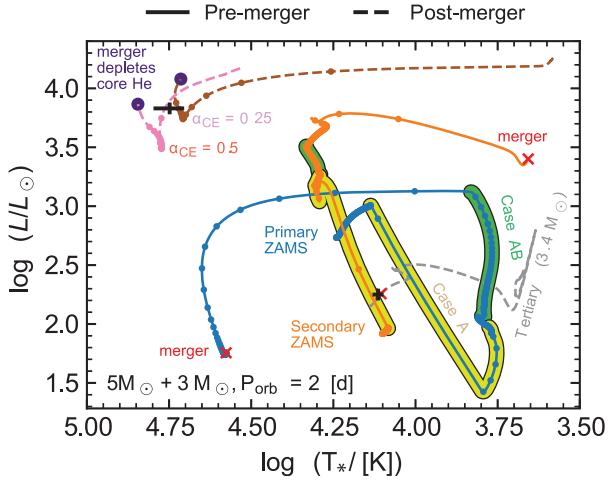

Fig. 5. Models of our proposed evolutionary scenario for HD 45166. MESA models are plotted on a temperature-luminosity diagram for a triple system. The inner binary comprises stars with masses of $5M_\odot$ (primary, blue line) and $3M_\odot$ (secondary, orange line), with an initial orbital period of 2 days. These tracks start from the zero-age main sequence (ZAMS). The outer tertiary star (gray line) has an initial mass of $3.4M_\odot$. Solid lines indicate the evolution of the three components before the inner binary merges; dashed lines show the post-merger evolution. Dots along each track are separated by 0.1 Myr of evolution. The merger is marked with a red cross. Colored regions indicate mass transfer on the main sequence (case A, yellow) and after the main sequence (case AB, green). The upper tracks indicate the evolution of the merger product (representing the Wolf-Rayet component) for assumed common-envelope ejection efficiencies of α_{CE} = 0.25 (brown) and 0.5 (pink) (*25*). The black plus signs indicate the observed properties of the Wolf-Rayet and B7 V components. Purple filled circles mark the core He depletion of the merger, which occurs after 133.2 and 133.7 Myr for α_{CE} = 0.25 and 0.5, respectively.

Wolf-Rayet component could be an immediate progenitor of a magnetar.

All magnetars in the Milky Way are isolated; they do not have a binary companion (*6*). For the Wolf-Rayet component in HD 45166, we expect the mass loss and velocity kick imparted on the magnetar by the supernova explosion to disrupt the system, given the large orbital separation. With an estimated rotation period of 125 d and an estimated radius of $\approx 0.3\,R_\odot$ for the helium core of the Wolf-Rayet component (*35*), angular-momentum conservation implies that the magnetar immediately after collapse would have a spin period $\lesssim$40 ms. This is similar to the spin period of the Crab Pulsar (33 ms), a neutron star that formed about 1000 years ago. Such a spin rate would not provide sufficient energy to power a superluminous supernova or a long-duration gamma-ray burst (*36*, *37*).

Evolutionary model of the system

We next considered how the Wolf-Rayet component itself formed. We excluded the possibly that it is the stripped core of a massive star, because to produce a 2 $M_\odot$ stripped core, the progenitor star would need to have had an initial mass of $\approx 10\,M_\odot$. Single-star evolution models do not predict that stars of that mass become stripped by mass loss (*22*, *38*), and the B7 V companion is too far away for binary interactions to have done so. In addition, the total lifetime (including post main-sequence evolution) of a 10 $M_\odot$ star would be ≈30 Myr (*39*), which is well below our derived age of the B7 V component (105 ± 35 Myr), so we reject the possibility that they could both be present in the same binary system.

Stellar mergers have been proposed as a potential origin of magnetic stars (*40*–*43*). Strong magnetic fields have been identified in low-mass helium stars (classified as OB-type subdwarfs) that have been suggested to originate from merger events between two white dwarfs (*13*, *14*). However, to produce a $\approx 2\,M_\odot$ helium star through a merger of white dwarfs, the merger would need to have involved massive CO or ONe white dwarfs, which are rare. Models predict that such a merger product would either immediately explode as a supernova (*44*) or do so after a short life span of approximately 10,000 years (*45*). We argue that observing the stellar product of a white-dwarf merger in the brief time available is unlikely.

We therefore propose that the Wolf-Rayet component in HD 45166 formed from the coalescence of the helium cores of two intermediate-mass stars that were bound in a close binary. We constructed an evolutionary model of this scenario (*25*) (Fig. 5) using the MESA stellar evolution code (*46*). We started the system in a triple configuration, with a tight inner binary and a distant tertiary star (the B7 V component). The model indicates

that the primary (more massive) star of the inner binary expanded and interacted with its companion, losing its outer layers and becoming a stripped star. Meanwhile, the companion (secondary star) accreted material and became rejuvenated with hydrogen. The secondary star later expanded itself, leading to an unstable mass-transfer back to the primary. In the model, this process leads to the formation of a gaseous envelope around the two stars, during which they both lose orbital energy owing to friction with the envelope, causing them to spiral inward (known as common-envelope evolution). Because of the high binding energy of the hydrogen-rich layers, this phase ends with both helium cores merging into a ≈2 $M_{\odot}$ magnetized helium star, while most (but not all) of the hydrogen envelope is ejected.

With a luminosity predicted to be 200 times that of a 2 $M_{\odot}$ main-sequence star (*47*), the merger product has a high luminosity-to-mass ratio. This, combined with its high effective temperature, launches a radiatively driven outflow from its surface. In the absence of a magnetic field, such an outflow would not be easily detectable in a spectrum. However, the trapping of an outflow by a magnetic field is known to increase the density of the circumstellar material and produce spectral emission lines, similar to those we observed in the Wolf-Rayet component (*26*, *48*). The distant tertiary star in our model does not affect the final outcome of the inner binary evolution, except perhaps by catalyzing the merging of its stellar components (*49*). Given its large orbital separation, we do not expect the tertiary star to show any evidence for accreted material from the merger ejecta.

Our proposed evolutionary scenario is quantitatively and qualitatively consistent with the observed properties of the system. The MESA model reproduces the masses of the two components and the estimated system age. The proposed merger provides an explanation for the emergence of a magnetic field in the Wolf-Rayet component, and the magnetic field provides an explanation for the presence of emission lines in the spectrum of a 2-$M_{\odot}$ helium star. The binary nature of HD 45166 enabled us to use the companion as a clock to constrain the evolutionary path of the system, and as a scale to determine the mass of the Wolf-Rayet component, which are conditions that are rarely present in other proposed merger products (*42*, *50*). Given the proximity of HD 45166 to Earth (≈1 kpc), other massive magnetic helium stars have likely already been spectroscopically identified as Wolf-Rayet stars but not recognized as magnetic (supplementary text).

REFERENCES AND NOTES

1. P. A. Crowther, *Annu. Rev. Astron. Astrophys.* **45**, 177–219 (2007).
2. N. Langer, *Annu. Rev. Astron. Astrophys.* **50**, 107–164 (2012).
3. B. Paczyński, *Acta Astron.* **17**, 355 (1967).
4. S. E. Woosley, *Astrophys. J.* **878**, 49 (2019).
5. E. Zapartas *et al.*, *Astron. Astrophys.* **601**, A29 (2017).
6. V. M. Kaspi, A. M. Beloborodov, *Annu. Rev. Astron. Astrophys.* **55**, 261–301 (2017).
7. S. Mereghetti, J. A. Pons, A. Melatos, *Space Sci. Rev.* **191**, 315–338 (2015).
8. L. Ferrario, A. Melatos, J. Zrake, *Space Sci. Rev.* **191**, 77–109 (2015).
9. L. Ferrario, D. Wickramasinghe, *Mon. Not. R. Astron. Soc.* **367**, 1323–1328 (2006).
10. G. A. Wade *et al.*, *Mon. Not. R. Astron. Soc.* **456**, 2–22 (2016).
11. J. H. Grunhut *et al.*, *Mon. Not. R. Astron. Soc.* **465**, 2432–2470 (2017).
12. A. de la Chevrotière, N. St-Louis, A. F. J. Moffat, *Astrophys. J.* **781**, 73 (2014).
13. M. Dorsch *et al.*, *Astron. Astrophys.* **658**, L9 (2022).
14. I. Pelisoli *et al.*, *Mon. Not. R. Astron. Soc.* **515**, 2496–2510 (2022).
15. M. E. Shultz, O. Kochukhov, J. Labadie-Bartz, A. David-Uraz, S. P. Owocki, *Mon. Not. R. Astron. Soc.* **507**, 1283–1295 (2021).
16. J. E. Steiner, A. S. Oliveira, *Astron. Astrophys.* **444**, 895–904 (2005).
17. W. R. Hamann *et al.*, *Astron. Astrophys.* **625**, A57 (2019).
18. Y. Götberg *et al.*, *Astron. Astrophys.* **615**, A78 (2018).
19. J. H. Groh, A. S. Oliveira, J. E. Steiner, *Astron. Astrophys.* **485**, 245–256 (2008).
20. J. S. Vink, *Astron. Astrophys.* **607**, L8 (2017).
21. A. A. C. Sander, J. S. Vink, *Mon. Not. R. Astron. Soc.* **499**, 873–892 (2020).
22. T. Shenar, A. Gilkis, J. S. Vink, H. Sana, A. A. C. Sander, *Astron. Astrophys.* **634**, A79 (2020).
23. N. R. Walborn, *Astron. J.* **77**, 312 (1972).
24. Y. Nazé *et al.*, *Astron. Astrophys.* **520**, A59 (2010).
25. Materials and methods are available as supplementary materials.
26. V. Petit *et al.*, *Mon. Not. R. Astron. Soc.* **429**, 398–422 (2013).
27. W. R. Hamann, G. Gräfener, *Astron. Astrophys.* **410**, 993–1000 (2003).
28. A. Sander *et al.*, *Astron. Astrophys.* **577**, A13 (2015).
29. F. R. N. Schneider *et al.*, *Astron. Astrophys.* **570**, A66 (2014).
30. J. F. Donati *et al.*, *Mon. Not. R. Astron. Soc.* **370**, 629–644 (2006).
31. G. A. Wade *et al.*, *Mon. Not. R. Astron. Soc.* **416**, 3160–3169 (2011).
32. G. Gräfener, J. S. Vink, A. de Koter, N. Langer, *Astron. Astrophys.* **535**, A56 (2011).
33. P. T. H. Pang *et al.*, *Astrophys. J.* **922**, 14 (2021).
34. R. C. Duncan, C. Thompson, *Astrophys. J.* **392**, L9 (1992).
35. N. Langer, Standard models of Wolf-Rayet stars. *Astron. Astrophys.* **210**, 93–113 (1989).
36. S. E. Woosley, *Astrophys. J. Lett.* **719**, L204–L207 (2010).
37. P. K. Blanchard, E. Berger, M. Nicholl, V. A. Villar, *Astrophys. J.* **897**, 114 (2020).
38. A. Maeder, G. Meynet, Stellar evolution with rotation. VI. The Eddington and Omega -limits, the rotational mass loss for OB and LBV stars. *Astron. Astrophys.* **361**, 159–166 (2000).
39. I. Brott *et al.*, *Astron. Astrophys.* **530**, A115 (2011).
40. L. Ferrario, J. E. Pringle, C. A. Tout, D. T. Wickramasinghe, *Mon. Not. R. Astron. Soc.* **400**, L71–L74 (2009).
41. D. T. Wickramasinghe, C. A. Tout, L. Ferrario, *Mon. Not. R. Astron. Soc.* **437**, 675–681 (2014).
42. F. R. N. Schneider *et al.*, *Nature* **574**, 211–214 (2019).
43. S. Bagnulo, J. D. Landstreet, *Astrophys. J. Lett.* **935**, L12 (2022).
44. R. F. Webbink, *Astrophys. J.* **277**, 355 (1984).
45. J. Schwab, E. Quataert, D. Kasen, *Mon. Not. R. Astron. Soc.* **463**, 3461–3475 (2016).
46. B. Paxton *et al.*, *Astrophys. J. Suppl. Ser.* **192** (Supp.), 3 (2011).
47. P. Harmanec, Stellar masses and radii based on modern binary data. *Bull. Astron. Inst. Czechoslov.* **39**, 329–345 (1988).
48. T. Shenar *et al.*, *Astron. Astrophys.* **606**, A91 (2017).
49. S. Toonen, S. Portegies Zwart, A. S. Hamers, D. Bandopadhyay, *Astron. Astrophys.* **640**, A16 (2020).
50. D. R. Gies, K. Shepard, P. Wysocki, R. Klement, *Astron. J.* **163**, 100 (2022).
51. T. Shenar, A massive helium star with a sufficiently strong magnetic field to form a magnetar, version 2, Zenodo (2023); https://doi.org/10.5281/zenodo.8040752.
52. powr-code/PoWR: v20220809, Zenodo (2022); https://doi.org/10.5281/zenodo.7217731.

ACKNOWLEDGMENTS

We thank the three anonymous referees for comments that improved the manuscript. The PoWR code was developed under the guidance of W.-R. Hamann with substantial contributions from L. Koesterke, G. Gräfener, A. Sander, T.S. and other coworkers and students. We thank J. Hessels, N. Przybilla, and H. Henrichs for helpful discussions. The TESS, IUE, and FUSE data were obtained from the Mikulski Archive for Space Telescopes (MAST) at the Space Telescope Science Institute (STScI), which is operated by the Association of Universities for Research in Astronomy under NASA contract NAS5-26555. T.S., P.M., L.O., and H.T. thank the International Space Science Institute (ISSI, Bern) for hosting a discussion meeting. NOIRLab is managed by the Association of Universities for Research in Astronomy (AURA) under a cooperative agreement with the National Science Foundation. This work is partly based on observations made with the Mercator Telescope, operated on the island of La Palma by the Flemish Community at the Spanish Observatorio del Roque los Muchachos of the Instituto de Astrofísica de Canarias. **Funding:** T.S. was supported by the European Union's Horizon 2020 Marie Skłodowska-Curie grant no. 101024605. D.M.B. and T.V.R. were supported by the Fonds Wetenschappelijk Onderzoek (FWO) through senior and junior postdoctoral fellowships under grant agreement nos. 1286521N and 12ZB620N, respectively. H.S. was supported by the European Research Council (ERC) under the European Union's Horizon 2020 research and innovation program (no. 772225: MULTIPLES). A.G. was supported by the Professor Amnon Pazy Research Foundation. N.S.-L. and G.A.W. received financial support from the Natural Sciences and Engineering Research Council (NSERC) of Canada. A.S.d.O. was supported by the FAPESP grant no. 03/12618-7. S.T. was supported by the Netherlands Research Council (NOW) grants VENI 639.041.645 and VIDI 203.061. Support to MAST for TESS, IUE, and FUSE data is provided by the NASA Office of Space Science through grant NAG5-7584 and by other grants and contracts. Funding for the TESS mission is provided by the NASA Explorer Program. T.S. acknowledges support from the Programa Atracción de Talento de la Comunidad de Madrid through grant 2022-T1/TIC-24117. **Author contributions:** T.S. developed the hypothesis, led the ESPaDOnS observations, performed the spectral and orbital analyses, and wrote the manuscript. G.W. performed the spectropolarimetric analysis and contributed to the observations and the manuscript. P.M. conceived the evolutionary scenario and constructed the corresponding MESA model. S.B. contributed to the spectropolarimetric analysis and to the manuscript. J.B. collected the HERMES data. D.M.B. and T.V.R. performed the light curve analysis. A.G. contributed to the evolutionary discussion and performed the population synthesis. N.L., S.T., and L.O. contributed to the discussion. A.N.-C., N.S.-L., and H.S. contributed to the observations, orbital analysis, and the data reduction. L.O. contributed to the discussion of magnetic Wolf-Rayet stars. H.S. contributed to the design of the observational campaign and the orbital analysis. N.S.-L. contributed to the design of the observational campaign. A.S.d.O. collected the LNA and FEROS observations. H.T. contributed to the spectral analysis. **Competing interests:** The authors declare no competing interests. **Data and materials availability:** Reduced and wavelength-calibrated FEROS, ESPaDOnS, LNA and HERMES spectra, the TESS light curve, the input and output files of our stellar evolution models, and the ZEEMAN source code are archived at Zenodo (*51*). The PoWR source code is available on GitHub https://github.com/powr-code/PoWR and archived at Zenodo (*52*). Our measured RVs are provided in data S1. The raw ESPaDOnS spectra are available on the CFHT archive www.cadc-ccda.hia-iha.nrc-cnrc.gc.ca/en/cfht under proposal ID 22BC13. The raw FEROS data are available on the ESO archive http://archive.eso.org/eso/eso_archive_main.html under target name HD 45166; we used the observations taken in 2002. The IUE data are available on MAST at https://archive.stsci.edu/iue/search.php under program IDs WRJSH, JA017, and EI273. The FUSE data are available on MAST at https://archive.stsci.edu/fuse/search.php under program ID P224. The raw TESS data are available on MAST at https://archive.stsci.edu/missions-and-data/tess with the coordinates of HD 45166; we used the data from full-frame images of sectors 6 and 33.

SUPPLEMENTARY MATERIALS

science.org/doi/10.1126/science.ade3293
Materials and Methods
Supplementary Text
Figs. S1 to S11
Tables S1 and S2
References (*53*–*110*)
Data S1

Submitted 10 August 2022; accepted 15 June 2023
10.1126/science.ade3293